

A Projective Phase Space Generator for Hadronic Vector Boson Plus One Jet Production

Tinghua Chen^a Terrance M. Figy^a and Walter T. Giele^b

^a*Department of Mathematics, Statistics, and Physics, Wichita State University, Wichita, Kansas, USA*

^b*Theory Group, Fermilab, Batavia, USA*

E-mail: txchen2@shockers.wichita.edu, terrance.figy@wichita.edu,
giele@fnal.gov

ABSTRACT: In this paper we use our previously developed projective phase space generator for the calculation of the hadronic production of a vector boson with one additional jet at Next-to-Leading Order. The projective phase space generator allows us to make physical predictions in novel ways, speeding up both evaluation time and attainable accuracy.

For the numerical evaluation, we explore a computational model which combines the use of both multi-threading and distributed resources through the use of grid or cloud computing without depending on local institutional computer availability. The projective phase space method is well suited for this approach and gives through the use of cloud computing instant access to a large pool of resources.

KEYWORDS: QCD, Hadron Colliders, LHC

ARXIV EPRINT: [1907.03893](https://arxiv.org/abs/1907.03893)

1 Introduction

The use of projective phase space methods opens up new ways to perform phase space integration at higher orders. The main advantage is the factorization of phase space into a physical Born phase space and a marginalized bremsstrahlung phase space. Any observable is defined on the Born phase space, while the bremsstrahlung phase space is integrated over with the constraint that the observables are unaltered. As a result, the radiative corrections are given as K -factors to the observable defined from the Born kinematics. The remaining challenge is connecting the Born defined observables with the experimental observables.

When this topic is discussed in the literature, it is typically from the viewpoint of the Matrix Element Method [1–8]. We follow a different approach as outlined in Ref. [9] where we view the topic as a simple phase space integration technique and consequently an issue of defining observables instead of the more restricted subject of Matrix Element Methods.

While constructing a projective phase space integration method is not particularly complicated, it becomes more involved when one wants to stay connected to a realistic experimental setting. Given a hadronic event, one can project this event to a unique Born event with a Leading Order (LO) weight using a jet algorithm. Any jet algorithm can be viewed as a projector of the hadronic event onto the partonic Born hard scattering event as it marginalizes out the particle content, thereby reducing the phase space dimensionality to the Born phase space dimensionality. Several issues will immediately arise, which will constrain a jet algorithm usable for a projective phase space integration method. First, a jet algorithm does not necessarily construct a massless 4-vector for the jet axis. Secondly, the reconstructed objects in the event are not necessarily balanced in transverse energy due to initial state radiation. The latter issue is specific for hadron colliders. Both these issues can cause problems for a perturbative prediction. An infrared stable jet algorithm should take these issues into consideration as the lowest order prediction has both massless jets and the objects in the event are strictly balanced in transverse momentum. The perturbative issues can be handled rigorously while the non-perturbative issues resulting from hadronization and the beam/proton remnants are the root of some fundamental issues that are more difficult to assess.

The addition of bremsstrahlung to a Born jet event makes changes to the event using traditional jet algorithms. One produces either an additional jet through wide angle hard branching, generate a p_T -imbalance in the reconstructed objects through initial state radiation or obtain a massive jet through soft/collinear final state branchings. The latter two types of branchings need to be integrated over, that is the radiation needs to be inclusive in order to obtain an infrared safe higher order prediction given the fixed Born event. Traditionally, one defines the observables using the reconstructed objects which in turn are constructed from events generated during a numerical integration over the bremsstrahlung phase space. This requires explicit finite width histogramming to combine the bremsstrahlung events with the virtual events to obtain the infrared safe prediction for the observable. Alternatively, one can specify the objects in advance and integrate over the radiation contributing to the fixed objects. This has the advantage one can define any observable using these inclusive objects

without the need to consider infrared stability as virtual corrections and bremsstrahlung have been properly combined at the object level without referring to either observable or explicit histogramming.

From the perspective of fixed higher order correction the inclusion of the bremsstrahlung directly into the object definition leads naturally to projective phase space techniques and the factorization into a Born phase space times a bremsstrahlung phase space. This results in many advantages over traditional phase space Monte Carlo integration techniques. While the integration over the jet mass is conceptually easy to understand, the treatment of the initial state radiation is more complicated. In Ref. [9] we developed a forward branching phase space (FBPS) generator which leaves key jet observables invariant with respect to the Born event. As a consequence any observable \mathcal{O} constructed from the final state objects and hence depending only on the Born kinematics can be calculated exclusively. That is, a Higher Order (HO) prediction of observable \mathcal{O} is given by a K -factor times the LO prediction, where $K(\mathcal{O})$ can be calculated order by order in perturbation theory without altering the observable \mathcal{O} . Note that these methods hark back to pre-Monte Carlo analytic phase space integration techniques (see e.g. [10]), but now implemented fully numerically offering all the flexibility coming with such an approach.

In Sec. 2 we discuss the definition of observables through an inclusive and exclusive jet algorithm at fixed order. We also discuss how to connect to realistic observables by including parton showers, hadronization and beam remnants. These methods are worked out in Sec. 4 for fixed order and in Sec. 5 for hadronized observables. Sec. 3 studies the slicing parameter dependence as we have not yet worked out a subtraction method compatible with the FBPS method. In Sec. 6 the ideas introduced in this paper are summarized.

2 Observables

At hadron colliders observables are usually built out of the boost invariant kinematic quantities of the reconstructed objects, namely transverse momentum, rapidity and azimuthal angle. Using these kinematic quantities to build observables enhances the infrared stability of these observables, while depending on other kinematic quantities which are not present at LO such as jet mass can cause infrared instabilities because they will in general constrain bremsstrahlung radiation.

The FBPS formalism projects events onto the Born kinematics and is constructed to predict observables using any infrared safe jet algorithm where the only restriction is that two clusters are combined sequentially by adding the respective 4-vectors of the two clusters. The projection is designed to leave the key kinematic quantities invariant. That is, the transverse momentum vector and rapidities of the observables are unaltered. These kinematic quantities completely fix the projected Born phase space point to a single event. Specifically, for the process $PP \rightarrow V + n$ jets, the FBPS formalism calculates the K -factor order-by-order in

pQCD for the maximum exclusive observable \mathcal{O}_{MAX}

$$\left. \frac{d\sigma}{d\mathcal{O}_{\text{MAX}}} \right|_{HO} = K(\mathcal{O}_{\text{MAX}}) \times \left. \frac{d\sigma}{d\mathcal{O}_{\text{MAX}}} \right|_{LO}$$

$$d\mathcal{O}_{\text{MAX}} = d\eta_V \times \prod_{i=1}^n \left(d\vec{p}_T^{(i)} d\eta_J^{(i)} \right), \quad (2.1)$$

point-by-point in phase space. (Note that we suppressed sums over partonic flavors for simplicity.) The transverse momentum vector and rapidity of jet i are given by $\vec{p}_T^{(i)}$ and $\eta_J^{(i)}$, respectively. The vector boson rapidity is given by η_V . Composite observables can be built from the maximal exclusive differential cross section. A noteworthy example is the value of the transverse momentum of the vector boson. At Born level this is constrained by momentum conservation $\vec{p}_T^V = -\sum_i \vec{p}_T^{(i)}$. At higher orders this becomes more complicated as not all final state partons are necessarily clustered into a jet $\vec{p}_T^V + \vec{p}_T^{\text{UNC}} = -\sum_i \vec{p}_T^{(i)}$ where \vec{p}_T^{UNC} is the transverse momentum vector of the summed momenta of the unclustered partons. For the needed projection onto Born any \vec{p}_T^{UNC} generated by the jet algorithm needs to be added to the vector boson, while the longitudinal vector boson momentum is re-scaled to leave the vector boson mass invariant. Finally, we can swap the vector boson momentum with one of the jet momenta in Eq. 2.1 if needed for constructing a composite observable containing the vector boson, i.e. $(\vec{p}_T^V, \eta_V) \leftrightarrow (\vec{p}_T^{(k)}, \eta_J^{(k)})$. In practice the \vec{p}_T -imbalance is easily avoided at parton level.

We use an inclusive partonic jet algorithm which terminates when a set number of n clusters are obtained. No beam jet is constructed in this jet algorithm and all partons are clustered into the jet(s), i.e. $\vec{p}_T^V + \sum_i \vec{p}_T^{(i)} = 0$. For a partonic final state this jet algorithm works well and simplifies the Monte Carlo implementation of the FBPS formalism significantly. An exclusive partonic jet algorithm can be simply defined by adding a $(n+1)$ -jet veto on the inclusive jet algorithm. This means the FBPS will integrate over the jet cones and initial state radiation, while excluding the $(n+1)$ -jet region of phase space. We can e.g. choose an anti- k_T jet algorithm [11]. However, it will project to a perfectly balanced Born event. That is all partons are clustered into one of the jets. It is worth noting that we integrate the bremsstrahlung partons exactly over the n -jet phase space defined by the anti- k_T algorithm. Only the object reconstruction differs between partonic and hadronic as for the latter we can have unclustered hadrons.

Before being able to compare with experimental data we have to consider hadronization and more relevant the proton/beam remnants which themselves carry a color charge. This forces a hadronic jet algorithm to construct a beam jet to ensure the proton remnant hadronic contribution into the hard scattering content is minimized. By using the partonic jet algorithms defined above we can still connect to a realistic experimental environment through the inclusion of a shower Monte Carlo [12–14]. In the FBPS formalism all partonic final states contributing to a single (multi-) jet event with a specified jet final state are integrated over, resulting in Eq. 2.1. This means we can shower the jets using any LO matching for-

malism initiated from the projected Born event. The shower will repopulate the regions of bremsstrahlung phase space which were integrated out on the partonic level.

The result is for the inclusive partonic jet algorithm of a fully exclusive hadronic final state where all radiative corrections are contained in the K -factor weight. Because showers are unitary, the K -factor will not be altered. Any experimental jet algorithm can be applied to the now fully exclusive hadronic final state. This will recast the partonic jets into the hadronic jets and the partonic Born phase space point will be smeared around this point. The result is that an observable does not necessarily contribute to a single bin, but can spread over multiple bins. Yet the weight of this distribution is still given by Eq. 2.1 and one can simply sum over the generated list of (possibly unit-weight) LO events, re-weighted by the K -factor. The only requirement of the shower is that it is unitary. In this scenario we rely on the shower MC to generate the hard branchings to give us additional jets. We will, in Sec. 5 use the VINCIA plugin [15–17] to PYTHIA [14, 18] for this purpose as it is Matrix Element (ME) corrected. Without a ME improved shower for the first branching(s) this is not expected to work well.

Without a ME corrected shower we can improve the hadronic event generation by employing a MLM matching scheme [19]. This will truncate the wide angle radiation generated by the parton shower from the NLO inclusive $Z + n$ -jet sample and hence dynamically reducing the size of the overall K -factor. The vetoed inclusive $(n + 1)$ -jet phase space region will be repopulated by showered LO $Z + (n + 1)$ -jet events, thereby negating the necessity of the ME corrected shower. In this paper we will not explore this particular option any further.

We see that by using a projective phase space integration method we can use a theoretical partonic jet algorithm to project on the Born phase space and yet through the use of a unitary shower Monte Carlo recast the events as fully hadronic events which can be reconstructed using any experimental jet algorithm and apply detector effects. The K -factor of the fully hadronic event can be calculated using the FBPS formalism order-by-order in perturbative QCD. Note that a Monte Carlo integration over the showered and K -factor re-weighted LO events is needed as the events are smeared out.

As a first exploration of these concepts we look at $PP \rightarrow Z + 1$ jet where we use our partonic jet algorithms including the recasting to hadronic jet algorithms using a shower Monte Carlo. The K -factor for this process is calculated up to Next-to-Leading order (NLO) $\mathcal{O}(\alpha_S^2)$.

3 Validation of the Slicing Method

While the FBPS method does not require slicing, a compatible subtraction method needs to be developed. For now we use a slicing method which fits well within a FBPS approach. This method can be used without any modifications. We will take $PP \rightarrow V + 1$ jet production at NLO using a slicing method as implemented in the DYRAD parton level MC [20] for all numerical results in this paper.

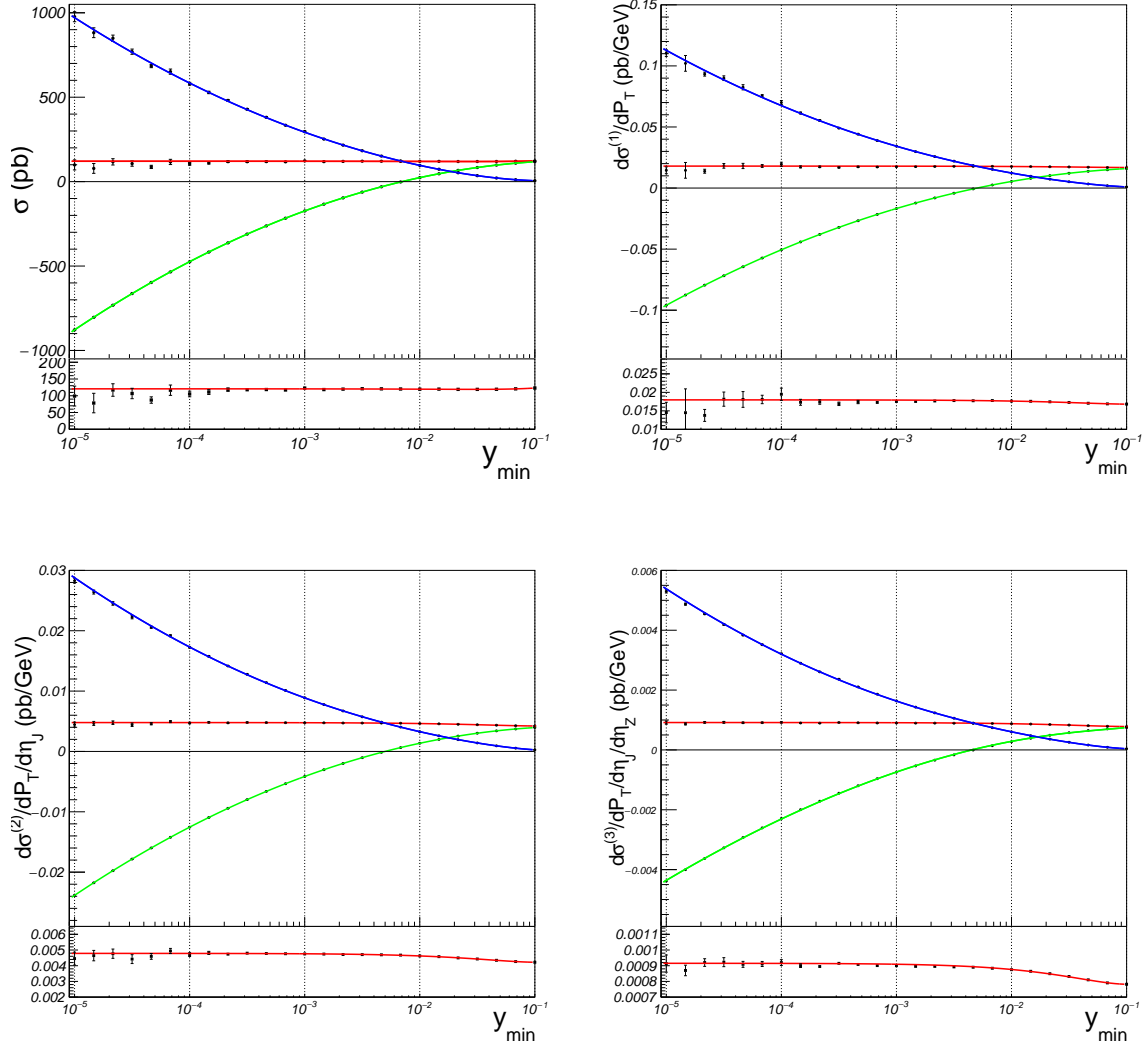


Figure 1. The y_{\min} dependence of the inclusive $PP \rightarrow Z + 1 \text{ jet}$ production at $\sqrt{S}=14$ TeV. Details are specified in text. The blue curve is the bremsstrahlung contribution, the green curves is the virtual contribution and the sum of the two contributions is represented by the red curve. The inclusive cross section is shown top left. The single differential distribution $d\sigma^{(1)}/dp_T^{\text{jet}}$ at $p_T^{\text{jet}} = 250$ GeV is shown top right. The double differential distribution $d\sigma^{(2)}/dp_T^{\text{jet}}/d\eta_{\text{jet}}$ at $p_T^{\text{jet}} = 250$ GeV and $\eta_{\text{jet}} = -0.75$ is shown bottom left. Finally, on the bottom right is the triple differential distribution $d\sigma^{(3)}/dp_T^{\text{jet}}/d\eta_{\text{jet}}/d\eta_Z$ at $p_T^{\text{jet}} = 250$ GeV, $\eta_{\text{jet}} = -0.75$ and $\eta_Z = 0.51$.

As a validation of the method and behavior with respect to the slicing parameter we look at four observables with increasing final state exclusivity. For all the MC runs we use VEGAS [21] as implemented in the CUBA library [22]. The use of the CUBA library extends the

DYRAD MC to include multi-threading, speeding up the run-time considerably depending on the available threads. The results for the dependence on the slicing parameter of the four observables are shown in Fig. 1. We use a collider energy of $\sqrt{S} = 14$ TeV, the renormalization and factorization scales set to $\mu_R = \mu_F = \sqrt{\hat{s}}$ with \hat{s} defined as the partonic collision energy, and the CT14nlo PDF set [23]. Shown are the real and virtual contributions together with the sum of these two contributions. This combined result is fitted to the expected leading behavior of the slicing parameter $y_{\text{MIN}} = s_{\text{MIN}}/\hat{s}$ for observable \mathcal{O}

$$\mathcal{O}(y_{\text{MIN}}) = \mathcal{O}(0) \times \left(1 + (a_1 \times y_{\text{MIN}} + a_2 \times y_{\text{MIN}}^2) \times \log(y_{\text{MIN}}) + \dots\right), \quad (3.1)$$

where s_{MIN} is the minimal invariant mass between two partons during the bremsstrahlung phase space integration. For the MC run to calculate the virtual and bremsstrahlung cross sections we selected a target relative accuracy of 0.1% with an event cap of 10,000,000.

The first observable we consider is the inclusive cross section σ where the transverse jet momentum $p_T^{\text{JET}} > 50$ GeV and the jet rapidity $\eta_{\text{JET}} < 3$. This is a traditional (3+3)-dimensional phase space integration (3 dimensions for the Born phase space plus 3 dimensions for the bremsstrahlung phase space). The result is summarized in

$$\begin{aligned} \sigma_{\text{LO}} &= (1.028 \pm 0.001) \times 10^2 \text{ pb} \\ \mathcal{O}(0) = \sigma_{\text{NLO}} &= (1.207 \pm 0.003) \times 10^2 \text{ pb}, \end{aligned} \quad (3.2)$$

where the fitting parameters are given $a_1 = 0.21 \pm 0.01$ and $a_2 = -3.0 \pm 0.2$.

The second observable is the single differential p_T^{JET} cross section at $p_T^{\text{JET}} = 250$ GeV and $\eta_{\text{JET}} < 3$. This reduces the phase space dimensionality to (2+3) (2 dimensions for the Born phase space plus 3 dimensions for the bremsstrahlung phase space), resulting in

$$\begin{aligned} \left. \frac{d\sigma_{\text{LO}}^{(1)}}{dp_T^{\text{jet}}} \right|_{p_T^{\text{jet}}=250 \text{ GeV}} &= (1.318 \pm 0.001) \times 10^{-2} \text{ pb/GeV} \\ \mathcal{O}(0) = \left. \frac{d\sigma_{\text{NLO}}^{(1)}}{dp_T^{\text{jet}}} \right|_{p_T^{\text{jet}}=250 \text{ GeV}} &= (1.797 \pm 0.004) \times 10^{-2} \text{ pb/GeV}, \end{aligned} \quad (3.3)$$

where the fitting parameters are given by $a_1 = 0.41 \pm 0.03$ and $a_2 = -1.2 \pm 0.2$.

The dimensionality of the third observable is further reduced to (1+3). This observable is the double differential cross section at the point $p_T^{\text{JET}} = 250$ GeV and $\eta_{\text{JET}} = -0.75$ giving

$$\begin{aligned} \left. \frac{d\sigma_{\text{LO}}^{(2)}}{dp_T^{\text{jet}} d\eta_{\text{jet}}} \right|_{p_T^{\text{jet}}=250 \text{ GeV}, \eta_{\text{jet}}=-0.75} &= (3.296 \pm 0.003) \times 10^{-3} \text{ pb/GeV} \\ \mathcal{O}(0) = \left. \frac{d\sigma_{\text{NLO}}^{(2)}}{dp_T^{\text{jet}} d\eta_{\text{jet}}} \right|_{p_T^{\text{jet}}=250 \text{ GeV}, \eta_{\text{jet}}=-0.75} &= (4.785 \pm 0.006) \times 10^{-3} \text{ pb/GeV}, \end{aligned} \quad (3.4)$$

where the fitting parameters are given by $a_1 = 0.78 \pm 0.02$ and $a_2 = -2.5 \pm 0.1$.

Finally, we restrict the Born kinematics to a single event (apart from the trivial azimuthal event angle). This leaves the (0+3) variables describing the bremsstrahlung particle left to integrate over. The result is given by,

$$\begin{aligned} \left. \frac{d\sigma_{\text{LO}}^{(3)}}{dp_T^{\text{jet}} d\eta_{\text{jet}} d\eta_Z} \right|_{p_T^{\text{jet}}=250 \text{ GeV}, \eta_{\text{jet}}=-0.75, \eta_Z=0.51} &= (6.169 \pm 0.000) \times 10^{-4} \text{ pb/GeV} \\ \mathcal{O}(0) = \left. \frac{d\sigma_{\text{NLO}}^{(3)}}{dp_T^{\text{jet}} d\eta_{\text{jet}} d\eta_Z} \right|_{p_T^{\text{jet}}=250 \text{ GeV}, \eta_{\text{jet}}=-0.75, \eta_Z=0.51} &= (9.154 \pm 0.007) \times 10^{-4} \text{ pb/GeV} , \end{aligned} \quad (3.5)$$

where the fitting parameters are given by $a_1 = 0.97 \pm 0.01$ and $a_2 = -3.3 \pm 0.4$.

Given the accuracy of the MC runs (a 0.1% statistical uncertainty on the virtual and bremsstrahlung MC integrations), we choose as a default the value of $y_{\text{MIN}} = 10^{-3}$ for the remainder of the paper. Note that the more exclusive observables have a stronger dependence on y_{MIN} . The value chosen for the slicing parameter should be safe for any observable at this accuracy.

As an alternative to **VEGAS** we also tried **SUAVE** [22]. For $y_{\text{MIN}} > 10^{-4}$ no statistically significant differences were observed. Below this value **SUAVE** underestimates the value of the cross section. We therefore will use **VEGAS** as implemented in CUBA for the remainder of the paper.

4 Theoretical Predictions

Originally a theoretical study of a particular distribution at NLO consisted of a calculation of the observable by hand with the aid of a non-MC computer program. The constructed program was dedicated to the calculation of that particular observable/distribution at parton level. There was no parton level MC approach or binning, instead the program calculating the differential cross section was a mixture of analytic parts and some minor numerical integrations. It calculated the value of the differential cross section for a specified input value of the observable (see e.g. refs. [10, 24]). The drawback of such an approach is that it is rigid, i.e., the definition of the observable is unalterable. Even the smallest change in the observable would necessitate a new calculation. Also in order to be able to perform the calculation, certain simplifications had to be made with respect to the experimental definition of the observable. The needed computer resources were small and in-line with what was available during that time-frame.

These drawbacks and the continued rise in available computer resources eventually led to the advent of parton level MC programs (see e.g. refs. [25, 26]) where the user numerically defines the observable resulting in a great flexibility. Moreover, the parton level MC program could calculate any observable/distribution. It has the expected drawbacks of a MC approach and requires a large amount of computer resources to obtain a reasonable integration uncertainty on the observable. Also, more responsibility was required from the user to calculate

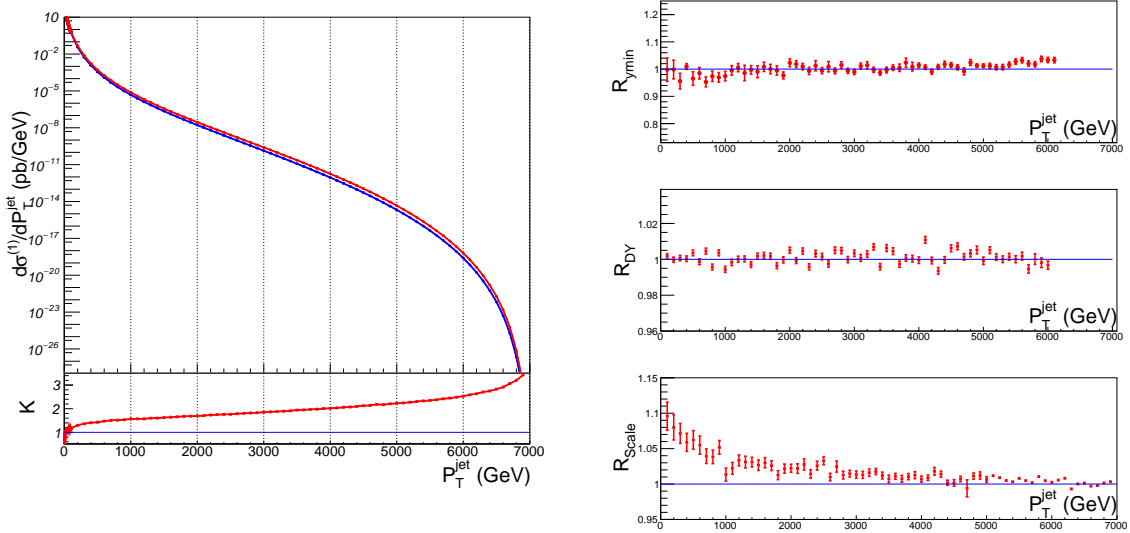


Figure 2. The transverse momentum distribution of the jet where $|\eta_{\text{jet}}| < 3$, $\mu_R = \mu_F = \sqrt{\hat{s}}$ and the parton density function CT14nlo is shown on the left. The blue line is the LO prediction and the red line is the NLO prediction. The ratio of the distribution for $y_{\min} = 10^{-4}$ over $y_{\min} = 10^{-3}$ is given in the top right figure, while the middle right figure shows the ratio of the FBPS MC over the original DYRAD MC. The bottom right figure shows the ratio of two different renormalization/factorization scale choices. See text for further details and discussion.

sensible, infrared safe observables. As the available computer power increased significantly over the last few decades this model was sustainable for more complicated NLO parton level MC's.

Because of technological limitations, currently different compute models are becoming more prominent. Multi-threading combined with the use of cloud distributed node farms seems to become the most efficient way to perform a computation. The need to calculate the differential cross section to ever more precision and for more and more complex observables only has accelerated this trend. The use of brute force MC integration of the partonic amplitudes using a simple phase space generator linked to an adaptive MC like **VEGAS** start to strain the available computer resources more and more. Because we could rely on ever more powerful CPU's in the last decades, numerical phase space integrations never evolved beyond what was used in parton level MC like [20, 26]. In contrast, the techniques and methods to calculate scattering amplitudes dramatically increased.

Here we apply the FBPS approach to combine the advantages of the original, more analytic approach and the parton MC approach within a framework of using multi-threading and cloud computing. To calculate distributions at parton level we can fully exploit the advantages of the FBPS approach. The distributions can be calculated on a finite grid of specific values of the observables without any binning. For the calculation of the differential

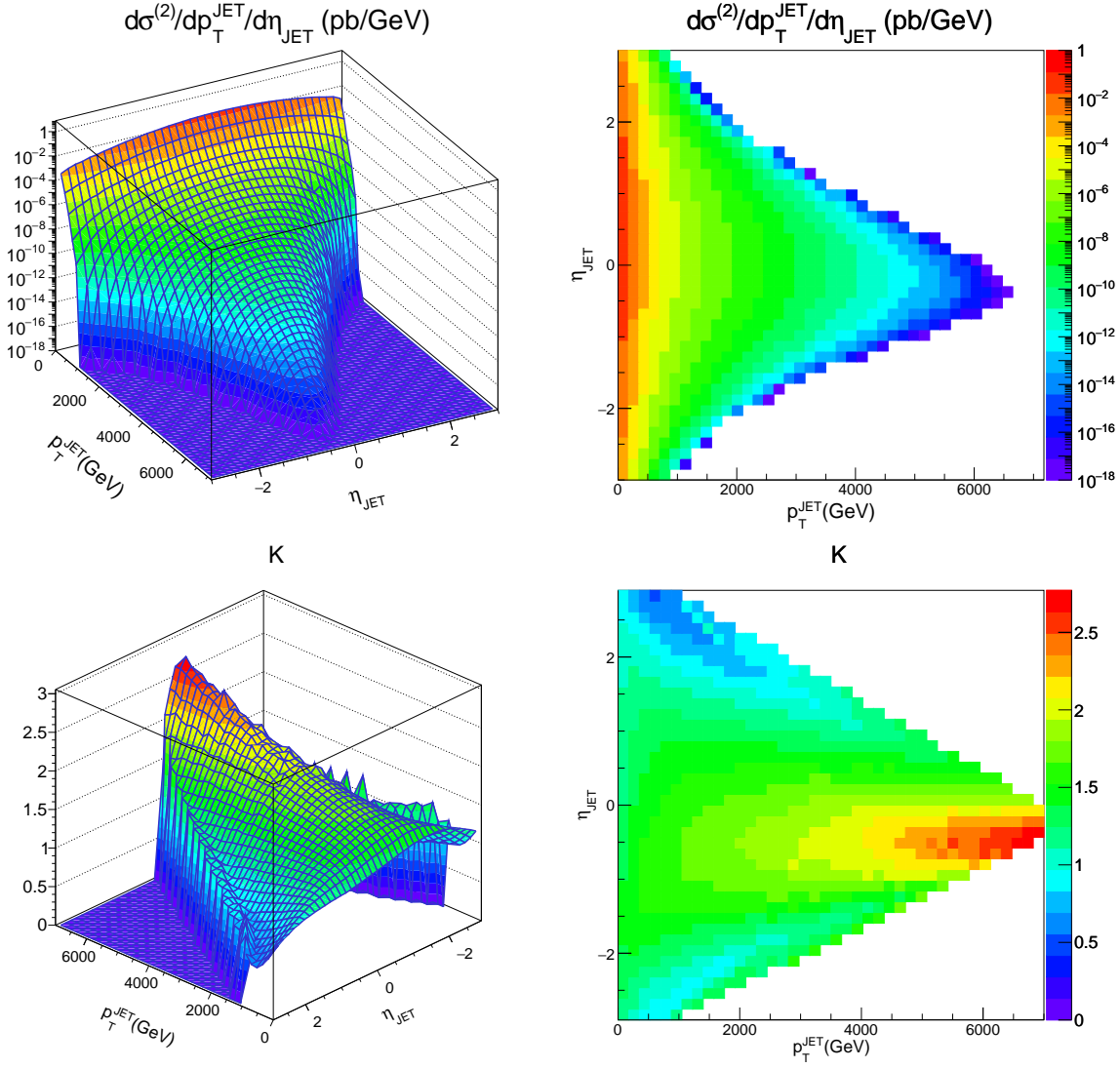


Figure 3. The 2-dimensional differential cross section (top row) and corresponding K -factor (bottom row) $d\sigma_{\text{NLO}}^{(2)}/dp_T^{\text{JET}}d\eta_{\text{JET}}$. The rapidity of the Z boson is fixed to $\eta_Z = 0.51$.

cross section, one can push each grid point to a different cloud node. This means we get precise predictions of the differential cross section for all chosen values of the observables in matter of minutes, independent of how many grid points we chose. At each value of the observable we can require a specific accuracy. Populating the entire range of possible values of the observable with the same relative integration uncertainty is trivial. We will use the Open Science Grid [27, 28] for our calculations.

As a first example we explore in Fig. 2 the transverse momentum distribution p_T^{JET} of the jet. Given our inclusive partonic jet algorithm which clusters all partonic particles into the jet,

the transverse momentum of the jet is almost identical to the transverse momentum distribution of the Z -boson, was it not for the rapidity cut on the jet. Because we fix the transverse momentum at a predetermined range of values, $p_t^{\text{JET}} = 1, 2, \dots, 99, 100, 200, \dots, 6800, 6900$ GeV, integrate over the remaining LO 2-dimensional phase space and subsequently calculate the K -factor by integrating over 3-dimensional bremsstrahlung phase space, we have excellent control over the integration accuracy at each p_T^{JET} point selected. We chose the relative integration accuracy for this distribution to be no larger than 0.1%. Additionally we can farm out each of the points to the grid. The results for the LO and NLO differential cross sections are shown in Fig. 2, together with the ratio of the NLO and LO differential cross section given by the K -factor,

$$\frac{d\sigma_{\text{NLO}}^{(1)}}{dp_T^{\text{JET}}} = K(p_T) \times \frac{d\sigma_{\text{LO}}^{(1)}}{dp_T^{\text{JET}}} . \quad (4.1)$$

The K -factor at both endpoints diverge as the bremsstrahlung is inhibited approaching $p_T^{\text{JET}} \rightarrow 0$ GeV and $p_T^{\text{JET}} \rightarrow 7000$ GeV. Away from the endpoints the K -factor gradually grows with increasing transverse momentum between the negative divergence as $p_T^{\text{JET}} \rightarrow 0$ GeV and the positive divergence as $p_T^{\text{JET}} \rightarrow 7000$ GeV. Because we do not need to bin event weights from randomly generated phase space point and can fix the p_T^{JET} value we have excellent control over the precision of the prediction at any p_T^{JET} -value of the jet. This is in sharp contrast to generic MC approaches where populating certain transverse momentum bins is complicated and maintaining a good accuracy over the entirety of the distribution is time expensive.

To validate slicing parameter independence we shown in Fig. 2 the ratio of the p_T -distribution choosing the slicing parameter 10^{-4} over the choice of 10^{-3} . As is shown the choice of the slicing parameter has no effect on the prediction and only affects the run time to reach the required integration uncertainty.

As a final check on the predictions we check the binned prediction of the original DYRAD MC to the FBPS version. To obtain the FBPS binned prediction we calculate

$$\left. \frac{\Delta\sigma}{\Delta p_T^{\text{JET}}} \right|_{p_T^{\text{MIN}} < p_T^{\text{JET}} < p_T^{\text{MAX}}} = \frac{\sigma(p_T^{\text{JET}} > p_T^{\text{MIN}}) - \sigma(p_T^{\text{JET}} > p_T^{\text{MAX}})}{p_T^{\text{MAX}} - p_T^{\text{MIN}}} . \quad (4.2)$$

As shown, the FBPS MC agrees well with the traditional parton level MC generator.

A final consideration is the renormalization/factorization scale choice. We have chosen the scale to be the partonic center-of-mass energy $\sqrt{\hat{s}}$. This is in principle an incorrect choice as we should construct the scale from the kinematics of the observables, i.e. the Born kinematics. Such a choice would make the scale and hence α_S a constant when integrating over the bremsstrahlung phase space. Constructing the Born equivalent of the partonic center-of-mass energy is readily done

$$\begin{aligned} \hat{s}^{\text{LO}} &= x_1^{\text{LO}} \times x_2^{\text{LO}} \times S \\ \sqrt{S} \times x_{1/2}^{\text{LO}} &= p_T^{\text{JET}} \times e^{\pm\eta_{\text{JET}}} + \sqrt{(p_T^V)^2 + M_V^2} \times e^{\pm\eta_V} . \end{aligned} \quad (4.3)$$

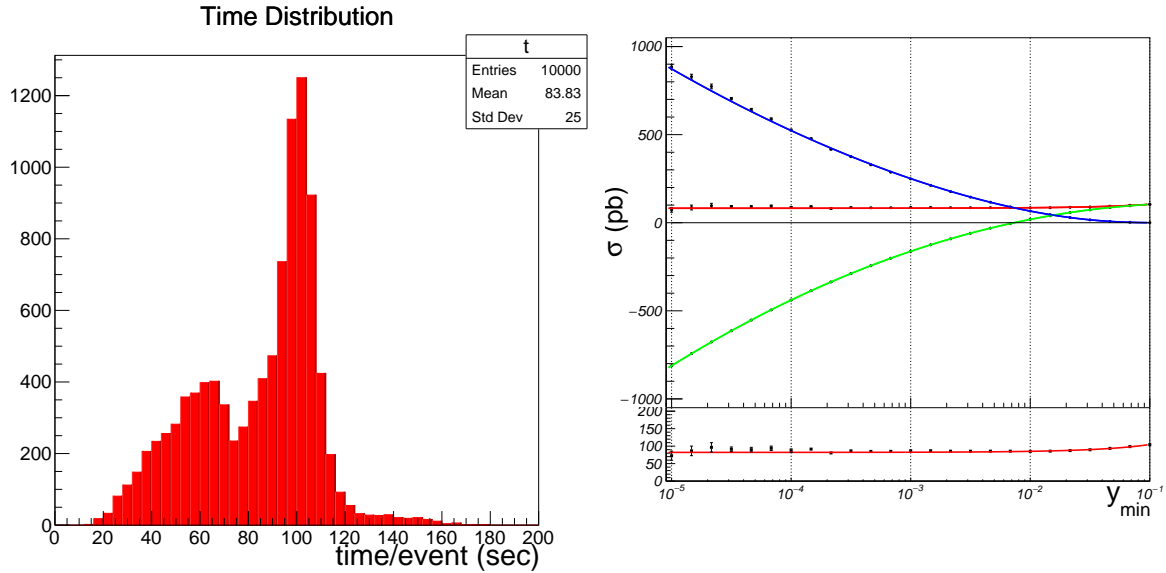


Figure 4. The runtime per event on the Open Science Grid of 10,000 batches of 100 events for a total of 1,000,000 events is shown in the left graph. The right graph gives the y_{\min} -dependence of the exclusive 1-jet cross section resulting in a integrated cross section of 82.2 ± 0.2 pb.

Note that $\hat{s} > \hat{s}^{\text{LO}}$ for any Born configuration. In Fig. 2 we show the ratio of the NLO differential cross section using the two scales and see that the difference is inconsequential. Although the LO partonic invariant mass gives a slightly flatter K -factor we will use the more intuitive choice of $\sqrt{\hat{s}}$ for the remainder of this section.

A 2-dimensional distribution can be calculated efficiently by extending the grid and by utilizing the cloud since the computational time is the same as for the 1-dimensional distribution. As an example we show in Fig. 3 the 2-dimensional NLO distribution and K -factor

$$\left. \frac{d\sigma_{\text{NLO}}^{(2)}}{dp_T^{\text{JET}} d\eta_{\text{JET}}} \right|_{\eta_Z=0.51} = K(p_T^{\text{JET}}, \eta_{\text{JET}}) \left. \frac{d\sigma_{\text{LO}}^{(2)}}{dp_T^{\text{JET}} d\eta_{\text{JET}}} \right|_{\eta_Z=0.51} \quad (4.4)$$

where the Z -boson rapidity is fixed to a value $\eta_Z = 0.51$ and transverse momentum and jet rapidity grids are given by $p_T^{\text{JET}} = 100, 200, \dots, 6200$ GeV and $\eta_{\text{JET}} = -3.0, -2.9, -2.8, \dots, 3.0$ resulting in a 61×61 2-dimension grid of points to be calculated for the distribution. The results show a rich phenomenology with large K -factors near the kinematic boundaries.

5 Connecting to the Experimental Observables

In the previous section we used the FBPS method on the parton level with the theoretical inspired inclusive jet algorithm. While this is somewhat esoteric, a study using this framework exposes the underlying phenomenology of the hard scattering process of interest to explore and understand. This contains all information of the physics we can extract from the measurement

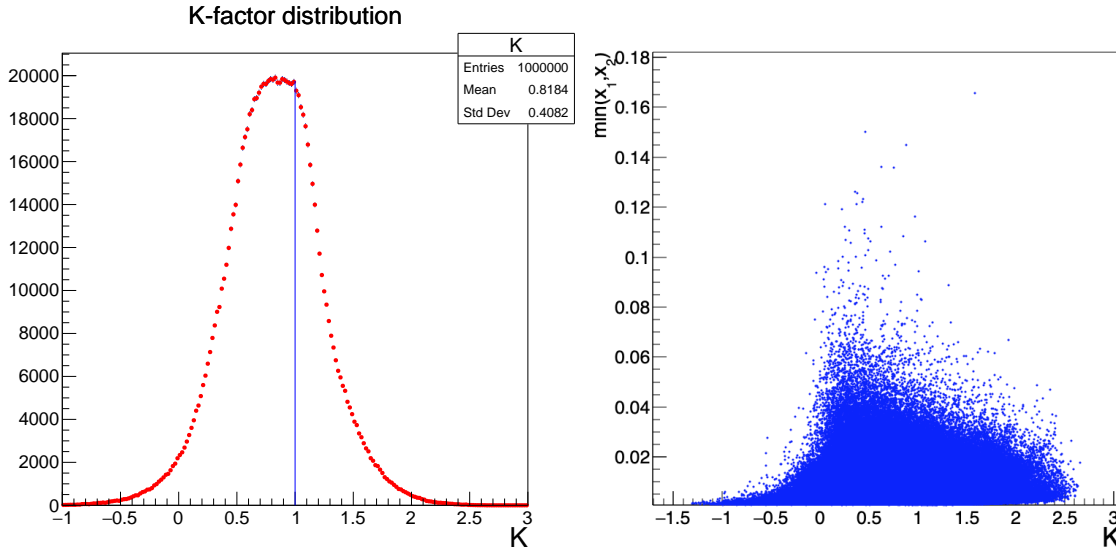


Figure 5. The K -factor distribution of 1,000,000 unit-weight LO events on the left. The graph on the right shows the relation between the K -factor and the smallest of the parton fractions in a scatter plot.

and is useful to both theorists and phenomenologists. To connect to the physical process as observed by experimenters we need to implement hadronization of the partonic state, including the recasting of the partonic jet algorithm into the hadronic jet algorithm with the main difference between the two being the beam remnant treatment which is absent for partonic jet algorithms. One can consider an analytic approach as is outlined in Ref. [29] which should give valuable insights into the hadronization process. However, to directly connect to the experimental measurements one has to use a parton shower with its subsequent hadronization and inclusion of the beam remnants.

As described in Sec. 2 we will implement an inclusive partonic jet showering approach for generating the hadronic sample of $PP \rightarrow Z + (\geq)1$ jets events. Before starting this analysis it is informative to have a look at some generic properties relevant for the production of large event samples. Both inclusive and exclusive jet algorithm methods start from a sample of 1,000,000 unit-weighted LO $PP \rightarrow Z + 1$ jet events which we generated using Madgraph [30, 31] for a collider energy of $\sqrt{S} = 14\text{TeV}$. For each of these events we need to calculate the K -factor which depends on the chosen jet algorithm. In Fig. 4 we show the run times for calculating the K -factors using the Open Science Grid. We submitted 10,000 jobs each containing 100 events to the cloud for a total of 1,000,000 calculated K -factors. As can be seen the evaluation time ranges over quite a large range. The run-time depends on the properties of the specific node which can vary. The figure shows the average run-time per event, indicating that if we use 1,000,000 cloud nodes simultaneously the calculation would be done in minutes. Instead we used 100 events per cloud node, reducing the number of required

nodes to 10,000. This means the overall run-time is of order hours, still sufficiently fast for a quick turn-around. Also shown in Fig. 4 is the slicing parameter y_{MIN} -dependence of the total cross section using the exclusive partonic jet algorithm with the cuts and K_T -algorithm parameter taken from the ATLAS paper of Ref. [32]. The slicing parameter dependence of various observables using the inclusive partonic jet algorithm were already given in Sec. 3.

The sample of hadronic events is generated using the inclusive partonic jet algorithm. To calculate the K -factors for each of the 1,000,000 unit-weight LO events we integrate over the full 3-dimensional bremsstrahlung phase space as the inclusive partonic jet algorithm does not depend on any parameters other than the number of final state clusters at which we stop clustering which in our case is one cluster. To get some feeling for the K -factors we show in Fig. 5 the distribution of K -factors. We see the mean K -factor is close to 1 as expected. We also see the K -factors can become negative for a small number of events. This is to be expected and to what extent this occurs depends on the cuts employed. To get some indication about the phase space regions which leads to negative K -factors we make a scatter plot using the $\min(x_1^{\text{LO}}, x_2^{\text{LO}})$. We see the negative K -factors are connected with small parton fraction events. These events are typically low transverse momentum, large rapidity events. The fact that negative K -factors exist makes re-weighting the LO events with the K -factors the best procedure. Interpreting the K -factors as some probability is not possible.

The showered final state sample is generated using the VINCIA shower Monte Carlo [15–17]. The subsequent analysis of the events was performed using RIVET [33]. Jets are reconstructed using the Anti- K_T jet algorithm with $R = 0.4$ [11] using FASTJET [34]. At least one jet with $p_T > 30$ GeV was required in a rapidity range of $[-5, 5]$. Leptons are required to have transverse momentum of $p_T > 10$ GeV and pseudo-rapidity in the range of $[-3.5, 3.5]$. Events where the invariant mass of a electron and positron between 71 GeV and 111 GeV are accepted, i.e., a single Z -boson is required. Besides the pQCD LO and NLO predictions we also show in Fig. 6 the results by showering the unit-weight LO events and applying the inclusive K -factor to obtain the showered NLO results. When applying the K -factor to the showered LO event we explore the most basic matching scheme. By applying the K -factor to the LO events we integrate the bremsstrahlung over the allowed phase space. That is, the clustered partons have the same transverse momentum vector and rapidity as the originating LO jet. We use the parton shower to refill the integrated out bremsstrahlung phase space with partons. This is per definition unitary as the shower is unitary. The entirety of the resulting 1-jet inclusive sample is at pQCD order α_S^2 enhanced by a Leading Log shower as the VINCIA shower is ME corrected.

In Fig. 7, we compare our showered LO and NLO $Z + 1$ jet results against the measured differential cross section from 3.16 fb^{-1} of ATLAS data at the CERN Large Hadron Collider experiment for the transverse momentum for the leading jet p_T^{jet} for events with one or more jets (inclusive) and one jet (exclusive) [32]. Note that we have made node effort to tune VINCIA or the renormalization and factorization scales involved in the calculation of the K -factor. In a future paper, we plan to perform a more careful comparison to all available experimental collider data such as the measured Z boson plus jets production cross section

for proton-proton collisions at $\sqrt{S} = 8$ TeV [35].

Because of the jet recasting we can use the theoretical motivated inclusive partonic jet algorithm which quite naturally has no knowledge of hadronization and beam remnants. Such physics is introduced by the shower MC in our approach. This recasts the jet from a partonic object to a fully hadronic object including physics like out of cone radiation and initial state radiation while at the same time preserving the pQCD K -factor of the event which is obtained by integrating over all possible decays of the event. Note that the hadronic sample requires no additional resolution parameters beyond the LO $Z + 1$ -jet generation of unit weight events. The only difference between LO shower (possibly detector corrected) sample and NLO is the K -factor reweighting. The K -factor is calculated at the parton level and can be outsourced to a cloud/farm environment. This trivially implies unitarity preservation, with the physical caveat of the $Z + 0$ -jet final state.

6 Conclusions

In this paper we revisited the fundamentals of the phase space integration needed to calculate higher order corrections for jet events at colliders. This results in new methods to make predictions in pQCD. The method is well suited for farm/cloud computing and gives access to large resources of computer power through, for example, the Open Science Grid without the need of gaining access to overburdened institutional computer resources. The reason goes back to the matrix element approach origins of the FBPS method. The calculation is partitioned in individual events, each can be outsourced to the cloud. Each partition involves the calculation of a single Born event plus its virtual corrections and the integration of the bremsstrahlung events of the partonic configurations over the phase space regions dictated by the partonic jet algorithm. The dimensionality of the bremsstrahlung phase space does not depend on the jet multiplicity, and is given by three times the number of bremsstrahlung partons involved, giving just a 3-dimensional integration at NLO. The jet multiplicity partitions phase space and sets up sectors to integrate over, i.e. one sector per jet. This does not affect the dimensionality, but will require more MC events to accurately cover all the sectors with sufficient number of events. Because of the low dimensionality at NLO, one can consider integration methods not based on the Monte Carlo integration.

We also made the first steps towards a full fledged method to construct Monte Carlo's in collider physics. It was shown that one can choose any partonic jet algorithm as long as it is infra-red safe and have summed four-vector sequential clustering. The partonic bremsstrahlung contributing to a fixed (multi-) jet configuration is integrated over, resulting in a K -factor to the Born amplitude. One can choose to let a shower Monte Carlo repopulate this region of phase space, recasting the partonic jet final state into a hadronic jet final state. The method generalizes readily beyond NLO, as the FBPS generator is branching based and therefore iterative like a parton shower.

The next steps are to extend the method to NNLO calculations and multi-jet final states. Furthermore the matching methods to parton showers need to be studied beyond the initial

steps in this paper so comparisons to existing data can be made.

Acknowledgments

T. F. acknowledges the kind support of the Fermi Theory Group. T. F. thanks Robert Kolleck for conversations concerning the splitting of event files. W. G. is supported by the DOE contract DE-AC02-07CH11359.

This research was performed using resources provided by the Open Science Grid, which is supported by the National Science Foundation and the U.S. Department of Energy’s Office of Science.

References

- [1] J. Alwall, A. Freitas and O. Mattelaer, *The Matrix Element Method and QCD Radiation*, *Phys. Rev.* **D83** (2011) 074010 [[1010.2263](#)].
- [2] W. T. Giele, G. C. Stavenga and J.-C. Winter, *A Forward Branching Phase-Space Generator*, [1106.5045](#).
- [3] J. M. Campbell, W. T. Giele and C. Williams, *The Matrix Element Method at Next-to-Leading Order*, *JHEP* **11** (2012) 043 [[1204.4424](#)].
- [4] J. M. Campbell, W. T. Giele and C. Williams, *Extending the Matrix Element Method to Next-to-Leading Order*, in *Proceedings, 47th Rencontres de Moriond on QCD and High Energy Interactions: La Thuile, France, March 10-17, 2012*, pp. 319–322, 2012, [1205.3434](#).
- [5] J. M. Campbell, R. K. Ellis, W. T. Giele and C. Williams, *Finding the Higgs boson in decays to $Z\gamma$ using the matrix element method at Next-to-Leading Order*, *Phys. Rev.* **D87** (2013) 073005 [[1301.7086](#)].
- [6] T. Martini and P. Uwer, *Extending the Matrix Element Method beyond the Born approximation: Calculating event weights at next-to-leading order accuracy*, *JHEP* **09** (2015) 083 [[1506.08798](#)].
- [7] T. Martini and P. Uwer, *The Matrix Element Method at next-to-leading order QCD for hadronic collisions: Single top-quark production at the LHC as an example application*, *JHEP* **05** (2018) 141 [[1712.04527](#)].
- [8] M. Kraus, T. Martini and P. Uwer, *Predicting event weights at next-to-leading order QCD for jet events defined by $2 \rightarrow 1$ jet algorithms*, [1901.08008](#).
- [9] T. M. Figy and W. T. Giele, *A forward branching phase space generator for hadron colliders*, *JHEP* **10** (2018) 203 [[1806.09678](#)].
- [10] S. D. Ellis, Z. Kunszt and D. E. Soper, *The One Jet Inclusive Cross-section at Order α_s^3 Quarks and Gluons*, *Phys. Rev. Lett.* **64** (1990) 2121.
- [11] M. Cacciari, G. P. Salam and G. Soyez, *The anti- k_t jet clustering algorithm*, *JHEP* **04** (2008) 063 [[0802.1189](#)].
- [12] M. Bahr et al., *Herwig++ Physics and Manual*, *Eur. Phys. J.* **C58** (2008) 639 [[0803.0883](#)].
- [13] T. Gleisberg, S. Hoeche, F. Krauss, M. Schonherr, S. Schumann, F. Siegert et al., *Event generation with SHERPA 1.1*, *JHEP* **02** (2009) 007 [[0811.4622](#)].

- [14] T. Sjöstrand, S. Ask, J. R. Christiansen, R. Corke, N. Desai, P. Ilten et al., *An Introduction to PYTHIA 8.2*, *Comput. Phys. Commun.* **191** (2015) 159 [[1410.3012](#)].
- [15] W. T. Giele, D. A. Kosower and P. Z. Skands, *A simple shower and matching algorithm*, *Phys. Rev.* **D78** (2008) 014026 [[0707.3652](#)].
- [16] W. T. Giele, D. A. Kosower and P. Z. Skands, *Higher-Order Corrections to Timelike Jets*, *Phys. Rev.* **D84** (2011) 054003 [[1102.2126](#)].
- [17] N. Fischer, S. Prestel, M. Ritzmann and P. Skands, *Vincia for Hadron Colliders*, *Eur. Phys. J.* **C76** (2016) 589 [[1605.06142](#)].
- [18] T. Sjostrand, S. Mrenna and P. Z. Skands, *PYTHIA 6.4 Physics and Manual*, *JHEP* **05** (2006) 026 [[hep-ph/0603175](#)].
- [19] M. L. Mangano, M. Moretti, F. Piccinini and M. Treccani, *Matching matrix elements and shower evolution for top-quark production in hadronic collisions*, *JHEP* **01** (2007) 013 [[hep-ph/0611129](#)].
- [20] W. T. Giele, E. W. N. Glover and D. A. Kosower, *Higher order corrections to jet cross-sections in hadron colliders*, *Nucl. Phys.* **B403** (1993) 633 [[hep-ph/9302225](#)].
- [21] G. P. Lepage, *A New Algorithm for Adaptive Multidimensional Integration*, *J. Comput. Phys.* **27** (1978) 192.
- [22] T. Hahn, *CUBA: A Library for multidimensional numerical integration*, *Comput. Phys. Commun.* **168** (2005) 78 [[hep-ph/0404043](#)].
- [23] A. Buckley, J. Ferrando, S. Lloyd, K. Nordström, B. Page, M. Rüfenacht et al., *LHAPDF6: parton density access in the LHC precision era*, *Eur. Phys. J.* **C75** (2015) 132 [[1412.7420](#)].
- [24] P. Nason, S. Dawson and R. K. Ellis, *The One Particle Inclusive Differential Cross-Section for Heavy Quark Production in Hadronic Collisions*, *Nucl. Phys.* **B327** (1989) 49.
- [25] H. Baer, J. Ohnemus and J. F. Owens, *A Next-to-leading Logarithm Calculation of Direct Photon Production*, *Phys. Rev.* **D42** (1990) 61.
- [26] W. T. Giele, E. W. N. Glover and D. A. Kosower, *The Two-Jet Differential Cross Section at $\mathcal{O}(\alpha_s^3)$ in Hadron Collisions*, *Phys. Rev. Lett.* **73** (1994) 2019 [[hep-ph/9403347](#)].
- [27] R. Pordes et al., *The Open Science Grid status and architecture*, *J. Phys. Conf. Ser.* **119** (2008) 052028.
- [28] I. Sfiligoi, D. C. Bradley, B. Holzman, P. Mhashilkar, S. Padhi and F. Wurthwein, *The pilot way to Grid resources using glideinWMS*, *WRI World Congress* **2** (2009) 428.
- [29] M. Dasgupta, L. Magnea and G. P. Salam, *Non-perturbative QCD effects in jets at hadron colliders*, *JHEP* **02** (2008) 055 [[0712.3014](#)].
- [30] J. Alwall, M. Herquet, F. Maltoni, O. Mattelaer and T. Stelzer, *MadGraph 5 : Going Beyond*, *JHEP* **06** (2011) 128 [[1106.0522](#)].
- [31] J. Alwall, R. Frederix, S. Frixione, V. Hirschi, F. Maltoni, O. Mattelaer et al., *The automated computation of tree-level and next-to-leading order differential cross sections, and their matching to parton shower simulations*, *JHEP* **07** (2014) 079 [[1405.0301](#)].

- [32] ATLAS collaboration, M. Aaboud et al., *Measurements of the production cross section of a Z boson in association with jets in pp collisions at $\sqrt{s} = 13$ TeV with the ATLAS detector*, *Eur. Phys. J.* **C77** (2017) 361 [[1702.05725](#)].
- [33] A. Buckley, J. Butterworth, L. Lonnblad, D. Grellscheid, H. Hoeth, J. Monk et al., *Rivet user manual*, *Comput. Phys. Commun.* **184** (2013) 2803 [[1003.0694](#)].
- [34] M. Cacciari, G. P. Salam and G. Soyez, *FastJet User Manual*, *Eur. Phys. J.* **C72** (2012) 1896 [[1111.6097](#)].
- [35] ATLAS collaboration, G. Aad et al., *Measurement of the inclusive cross-section for the production of jets in association with a Z boson in proton-proton collisions at 8 TeV using the ATLAS detector*, [1907.06728](#).

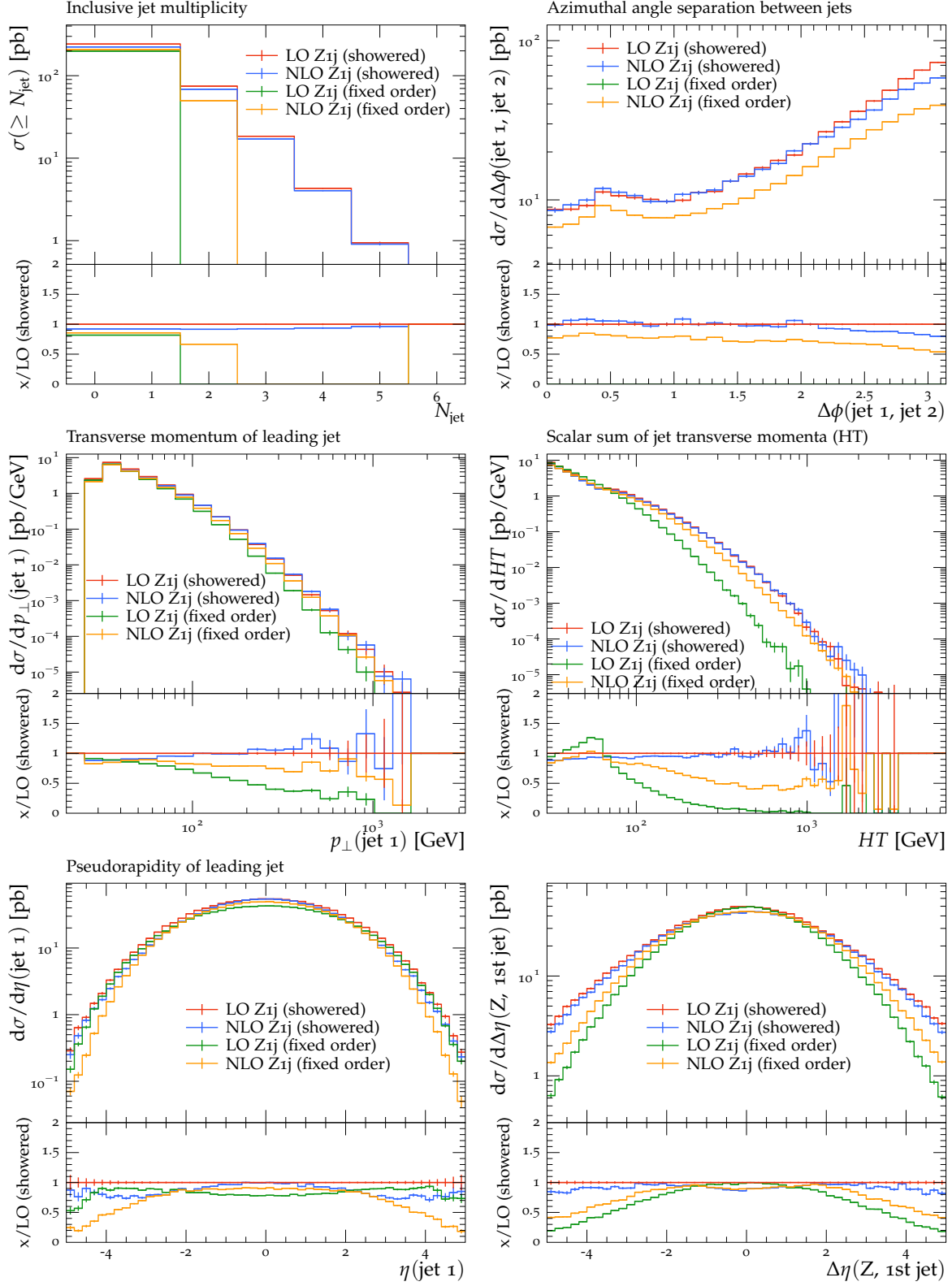


Figure 6. Shown are the pQCD LO (LO Z1j (fixed order)) and NLO (NLO Z1j (fixed order)) predictions. The inclusive showered results using VINCIA originating from the pQCD events LO Z1j (showered) and NLO Z1j (showered).

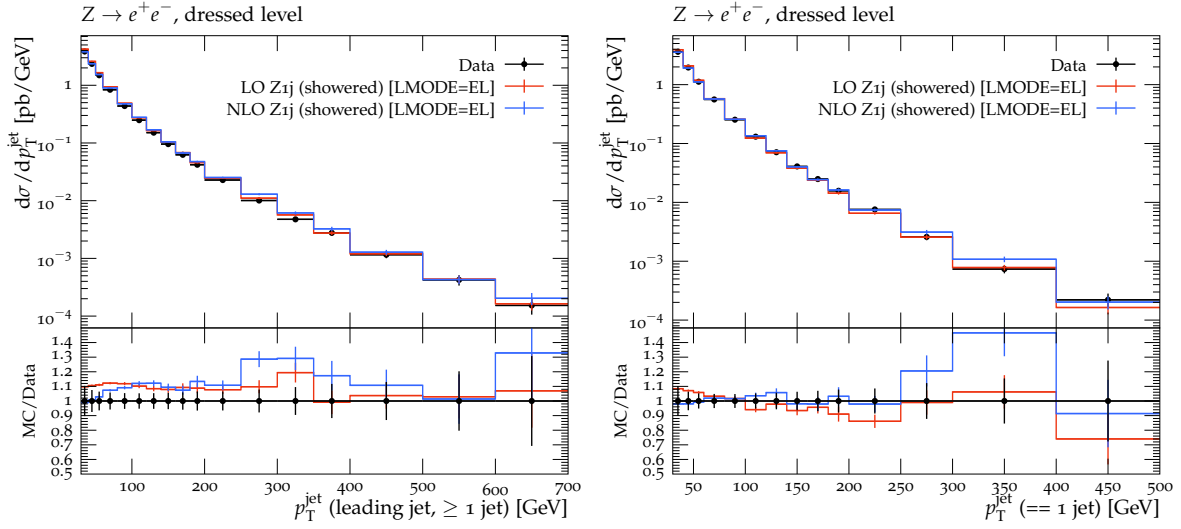


Figure 7. The inclusive showered results using VINCIA originating from the pQCD events LO Z1j (showered) and NLO Z1j (showered). Theory predictions are compared to the measured differential production cross sections from 3.16 fb^{-1} of ATLAS data at the CERN Large Hadron Collider for Z boson in association of jets in proton-proton collision at $\sqrt{S} = 13 \text{ TeV}$ [32].